Detection of deep stratospheric intrusions by cosmogenic ^{35}S

Mang Lin[a,1], Lin Su[b], Robina Shaheen[a], Jimmy C. H. Fung[c,d], and Mark H. Thiemens[a,1]

[a]Department of Chemistry and Biochemistry, University of California, San Diego, La Jolla, CA 92093; [b]Environmental Science Programs, School of Science, Hong Kong University of Science and Technology, Clear Water Bay, Hong Kong, China; [c]Division of Environment, Hong Kong University of Science and Technology, Clear Water Bay, Hong Kong, China; and [d]Department of Mathematics, Hong Kong University of Science and Technology, Clear Water Bay, Hong Kong, China

Edited by Barbara J. Finlayson-Pitts, University of California, Irvine, CA, and approved August 18, 2016 (received for review June 23, 2016)

The extent to which stratospheric intrusions on synoptic scales influence the tropospheric ozone (O_3) levels remains poorly understood, because quantitative detection of stratospheric air has been challenging. Cosmogenic ^{35}S mainly produced in the stratosphere has the potential to identify stratospheric air masses at ground level, but this approach has not yet been unambiguously shown. Here, we report unusually high ^{35}S concentrations (7,390 atoms m^{-3}; ∼16 times greater than annual average) in fine sulfate aerosols (aerodynamic diameter less than 0.95 μm) collected at a coastal site in southern California on May 3, 2014, when ground-level O_3 mixing ratios at air quality monitoring stations across southern California (43 of 85) exceeded the recently revised US National Ambient Air Quality Standard (daily maximum 8-h average: 70 parts per billion by volume). The stratospheric origin of the significantly enhanced ^{35}S level is supported by in situ measurements of air pollutants and meteorological variables, satellite observations, meteorological analysis, and box model calculations. The deep stratospheric intrusion event was driven by the coupling between midlatitude cyclones and Santa Ana winds, and it was responsible for the regional O_3 pollution episode. These results provide direct field-based evidence that ^{35}S is an additional sensitive and unambiguous tracer in detecting stratospheric air in the boundary layer and offer the potential for resolving the stratospheric influences on the tropospheric O_3 level.

stratosphere–troposphere exchange | surface ozone | National Ambient Air Quality Standard | radioactive isotope of sulfur | Santa Ana wind

High ground-level ozone (O_3) mixing ratios exert adverse impacts on human health, vegetation, and materials (1, 2). In the free troposphere, O_3 is an important greenhouse gas contributing to global warming. It also controls the lifetime of other reactive greenhouse gases through oxidation processes (3), serves as the dominant precursor of the hydroxyl radical, and enhances the oxidizing capacity of the troposphere (4). Tropospheric O_3 formation involves a series of photochemical reactions related to anthropogenic emissions of O_3 precursors [e.g., nitrogen oxides (NO_x), carbon monoxide (CO), and volatile organic compounds (VOCs)], biomass burning, and lightning (5). In addition, elevated levels of tropospheric O_3 may be caused by the intrusion of O_3-rich stratospheric air masses (4, 6–8). Detection of such stratospheric intrusion events by field-based measurements has been a major scientific concern since the 1970s (9). Concurrent measurement of ground-level O_3, CO, and humidity is the most common method (10, 11), but it is ambiguous and only useful in extreme events and background sites. Ozonesondes, lidar, and aircraft measurements provide high-resolution information on vertical O_3 distributions (12–14), but they are relatively expensive and not widely available. Therefore, it is crucial to find an additional and unambiguous stratospheric tracer at ground level to assist in such investigations.

^{35}S (half-life = 87 d) is a cosmogenic isotope naturally produced by the interaction of high-energy cosmic rays with ^{40}Ar in the atmosphere. The flux of cosmic rays and the production rate of ^{35}S depend on both latitude and altitude, with higher values at the polar region and in the stratosphere (and lower at the equatorial region and in the boundary layer) (15). Cosmogenic ^{35}S oxidizes to $^{35}SO_2$ in ∼1 s after production and is further oxidized to $^{35}SO_4^{2-}$ before wet and dry removal. Therefore, the variation of $^{35}SO_4^{2-}$ concentrations at ground level is controlled by the SO_2 oxidation and sulfate removal rates as well as air masses originating from the higher atmosphere. Because of the higher production rate of ^{35}S in the stratosphere (one to two orders of magnitude greater than in the troposphere) (15), significant enhancement of $^{35}SO_4^{2-}$ concentration at ground level may offer a new tool to quantify the impact of deep stratospheric intrusions on tropospheric O_3. A unique advantage of ^{35}S is that it exists in both gas (SO_2) and particle (sulfate) phases and has an ideal half-life (87 d) for studying atmospheric processes on synoptic scales, providing additional information on potential impacts of stratospheric intrusions on gas to particle (SO_2 to SO_4^{2-}) conversion rates. The development of the optimized low-level liquid scintillation counting technique (16) gave rise to a growing number of aerosol $^{35}SO_4^{2-}$ measurements in recent years. Based on simple and unconstrained 1D box model calculations, slightly elevated $^{35}SO_4^{2-}$ concentrations in early studies were linked to the polar vortex activity (17), Santa Ana winds, and shallow stratosphere–troposphere exchange events in southern California (18). Recent studies applied mesoscale meteorology models to investigate the possible downward transport processes of aged stratospheric air (19, 20). However, the reliability of ^{35}S as a stratospheric tracer remains uncertain and debated, because the magnitudes of $^{35}SO_4^{2-}$ enhancements were relatively small and

Significance

The recently revised stricter US National Ambient Air Quality Standard for ground-level ozone (O_3) requires precise methods to screen "exceptional events," such as naturally occurring deep stratospheric intrusions. However, existing approaches used in detecting stratospheric intrusions and evaluating their contributions to ground-level O_3 enhancement are not satisfactory. Here, we introduce the use of cosmogenic ^{35}S to assist in such quantifications. We measured the highest ^{35}S concentration in natural sulfate aerosols ever reported in the literature during deep stratospheric intrusions. The downward transport of stratospheric O_3 is confirmed by air quality data and meteorological analysis, showing the high sensitivity of ^{35}S as a stratospheric tracer and its utility to understand atmospheric transport and chemistry processes.

Author contributions: M.L., R.S., and M.H.T. designed research; M.L. and L.S. performed research; M.L., J.C.H.F., and M.H.T. contributed new reagents/analytic tools; M.L. and L.S. analyzed data; and M.L., L.S., R.S., and M.H.T. wrote the paper.

The authors declare no conflict of interest.

This article is a PNAS Direct Submission.

[1]To whom correspondence may be addressed. Email: m6lin@ucsd.edu or mthiemens@ucsd.edu.

This article contains supporting information online at www.pnas.org/lookup/suppl/doi:10.1073/pnas.1609919113/-/DCSupplemental.

Table 1. $^{35}SO_4^{2-}$ concentrations in size-segregated aerosol samples collected at the University of California, San Diego in spring of 2014

Date	Total airflow (m^3)	$^{35}SO_4^{2-}$ (atoms m^{-3})		
		>7.2 μm	0.95–7.2 μm	<0.95 μm
March 27 to April 4	11,647	12 ± 7	33 ± 5	90 ± 4
April 6 and 7	1,543	n.d.	n.d.	170 ± 40
April 12–18	9,503	15 ± 8	77 ± 6	230 ± 10
May 3–7	7,176	4 ± 6	75 ± 8	7,390 ± 50
May 10–14	7,571	n.d.	50 ± 10	370 ± 20
May 19–23	7,727	3 ± 7	51 ± 7	130 ± 10

n.d., Not detectable.

other stratospheric signatures (e.g., high O_3 level and low humidity) were not observed in suspected aged stratospheric air masses (18, 19). Measurements of $^{35}SO_4^{2-}$ during deep stratospheric intrusions, which directly entrain fresh stratospheric air to the boundary layer, have never been made.

Climatological studies showed that the western United States is one of the global hotspots for deep stratospheric intrusions, which is likely because of the east Pacific storm track and the high-altitude orography (4, 21). Such deep stratospheric intrusion events compromise high-altitude regions of the western United States in attaining US National Ambient Air Quality Standard (NAAQS) for O_3 (6). Additional field-based observation studies indicated that this O_3-rich stratospheric air can even be transported to low-altitude regions, such as Los Angeles at the southern California coast (8, 22, 23). Consequently, this region is a natural laboratory for studying the potential of ^{35}S as a tracer for stratospheric intrusions. In October of 2015, the NAAQS for O_3 was revised to 70 ppbv (parts per billion by volume) [daily maximum 8-h average (MDA8)] from the previous standard of 75 ppbv by the US Environmental Protection Agency (EPA). This new standard has been effective since December 28, 2015, and hence, identifying and excluding such naturally occurring "exceptional events" become increasingly important (24). The EPA recommends identifying exceptional events with supporting evidence, emphasizing the urgent need to find a new and sensitive stratospheric tracer, such as ^{35}S, to offer an unambiguous diagnostic for stratospheric intrusions. In this study, we measure ^{35}S concentrations during deep stratospheric intrusions to show the sensitivity of ^{35}S to stratospheric air in the boundary layer.

Field-Based ^{35}S Measurements

Table 1 summarizes ^{35}S concentrations in size-segregated sulfate aerosol ($^{35}SO_4^{2-}$) collected on the rooftop of Pacific Hall on the campus of the University of California, San Diego [32.876° N, 117.242° W; 120 m above sea level (a.s.l.)] in spring of 2014. Most of ^{35}S concentrations agree well with our previous measurements at the Scripps Pier (10 m a.s.l. and 1.7 km from the sampling site in this study) (18), but an unusually high $^{35}SO_4^{2-}$ concentration of 7,390 atoms m^{-3} was found in the fine aerosol sample (with aerodynamic diameter less than 0.95 μm) collected on May 3, 2014, ∼16 times greater than the annual mean of 460 atoms m^{-3} (18, 25) (Fig. 1). In fact, this value is the highest $^{35}SO_4^{2-}$ concentration ever reported for natural aerosol samples in the literature, which may be explained by stratospheric influence. It is noted that comparably high ^{35}S levels were measured in two rainwater samples collected in Korea in spring and winter (200 and 400 mBq L^{-1}, respectively), two seasons with frequent stratospheric intrusions in East Asia (26), which were significantly greater (more than a factor of ∼6) than other rainwater samples (4–60 mBq L^{-1}) (27). Using the $^{35}SO_4^{2-}$ scavenging ratio obtained in Japan (28), the atmospheric $^{35}SO_4^{2-}$ concentrations in Korea were calculated to be 150–2,200 atoms m^{-3} in most cases and 7,500 and 15,000 atoms m^{-3} in two episodes. Although this estimation is subject to large uncertainties (∼60% relative SD) (28), it matches the most recent $^{35}SO_4^{2-}$ measurement directly made on aerosol samples collected in East Asia (90–1,130 atoms m^{-3} in most samples and an increased $^{35}SO_4^{2-}$ concentration of 3,150 atoms m^{-3} in a sample affected by aged stratospheric air from the free troposphere) (20). The aforementioned high rainwater ^{35}S activities (27) were likely affected by stratospheric intrusions but were not considered. In this study, the stratospheric origin of our unusually high $^{35}SO_4^{2-}$ concentration directly measured on sulfate aerosol is examined.

Before discussing the impacts of stratospheric intrusions, other potential factors should be carefully evaluated. Apart from natural cosmogenic production, the $^{35}Cl[n,p]^{35}S$ reaction between neutrons escaping from Fukushima and ^{35}Cl in the coolant seawater is the only identified anthropogenic source of ^{35}S (25, 28). It is worthwhile to note that core elements reactors do not emit ^{35}S. It is high levels of ^{35}Cl in seawater that react with neutrons and allow ^{35}S productions. Given the highly specific reaction condition, there is no evidence showing that the observed $^{35}SO_4^{2-}$ spike in this study is caused by the $^{35}Cl[n,p]^{35}S$ reaction in the Fukushima or any nuclear plant. In addition, it was proposed that atmospheric $^{35}SO_4^{2-}$ removed by precipitation or dry deposition processes might reenter the boundary layer through the atmosphere and land surface interaction (biomass burning or wind-blown terrestrial dust) within ∼66 d and elevate $^{35}SO_4^{2-}$ concentrations in the boundary layer (27). Although this hypothesis remains to be proven, we carefully screen out this potential scenario. Large wildfires (>300 acres; defined by the California Department of Forestry and Fire Protection) were not recorded during the sampling period (cdfdata.fire.ca.gov/pub/cdf/images/incidentstatsevents_253.pdf). The absence of large wildfires is also supported by the satellite observations (Fig. S1). Therefore, any significant contribution of ^{35}S from biomass burning is implausible in this study period. The low $^{35}SO_4^{2-}$ concentration in coarse particle observed in the same set of aerosol samples (Table 1) also suggests that $^{35}SO_4^{2-}$ in resuspended terrestrial soil or dust cannot account for the notable enhancement of $^{35}SO_4^{2-}$ in this study. To date, there is no evidence or theory showing that other sources/processes can lead to significant variations or productions of ^{35}S. After considering all potential factors, the impact of air masses from the stratosphere, where the natural cosmogenic production rate of ^{35}S is approximately two orders of magnitude greater than the Earth's surface (15), is the most likely candidate to explain the elevated ^{35}S concentration.

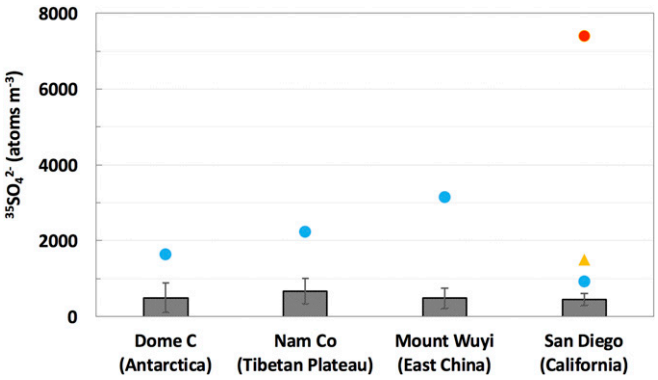

Fig. 1. The $^{35}SO_4^{2-}$ concentration in the fine aerosol sample collected on May 3, 2014 (red circle) and the comparison with annual means (gray bars; error bars stand for 1 SD) and the highest values (blue circles) measured at different sampling sites in previous studies (17–20). The orange triangle represents the sample affected by the trans-Pacific transport of ^{35}S produced from the $^{35}Cl[n,p]^{35}S$ reaction in Fukushima (25).

Exceptional Event of O_3 Enrichment

On May 3, 2014, when the ^{35}S-rich aerosol sample was collected, a regional O_3 pollution event was observed over southern California (Fig. 2). Two stations in Los Angeles were in the category of "unhealthy" [Air Quality Index (AQI): 151–200 or MDA8: 86–105 ppbv], and 80% of stations in southern California (68 of 85) were in the categories of "unhealthy for sensitive groups" (AQI: 101–150 or MDA8: 71–85 ppbv) or "moderate" (AQI: 51–100 or MDA8: 55–70 ppbv). Although the other 15 stations were in the category of "good" (AQI: 0–50 or MDA8: 0–54 ppbv) on this day, the O_3 mixing ratios in 14 stations were still higher than annual means, and five of them were significantly greater (>80th percentile) than normal days. The relatively low O_3 mixing ratios (compared with other stations) are because of substantial NO emissions from vehicles in surrounding areas that lower ambient O_3 mixing ratios via the "titration effect" ($NO + O_3 \rightarrow NO_2 + O_2$) (29). For example, the MDA8 of 54 ppbv in the Otay Mesa station (located at the United States–Mexico border and affected by the busy crossing of heavy-duty trucks) on May 3, 2014 was the annual highest value.

Fig. 3 *A* and *B* shows the time series of relative humidity (RH), temperature, and wind speed recorded in San Diego from April 27 to May 8, 2014. RH dramatically dropped down from 67% at 2100 hours Pacific Standard Time (PST) on April 28 to 7% at 1500 hours PST on April 29 accompanied with enhanced temperature (~30 °C) and wind speed (>15 m/s). The wind speed reached a maximum of 28 m s^{-1} on April 30, with wind direction shift from variable to northwesterly (Fig. 3*B*). These abnormal meteorological conditions are typical signatures of Santa Ana winds, which are highly dry, hot, and strong winds that descend from inland desert regions to the Pacific coastal region in southern California (18, 22, 30–32). These foehn-like katabatic winds result from a strong pressure gradient between a high pressure over the Great Basin and an offshore low pressure. The high pressure can compress sinked air, force the air temperature to rise, and reduce its RH. Although the wind speed returned back to normal on May 2, 2014, low RH and high temperature persisted until May 4, suggesting that the Santa Ana wind event lasted for 5 d (April 29 to May 3, 2014).

Santa Ana wind events are often behind a cold front associated with an upper-level trough (31), which cannot only exacerbate the katabatic winds but also, can lead to the formation of deep tropopause folds and stratospheric intrusions (22). A recent study suggested that the coupling between Santa Ana winds and stratospheric intrusions might pose serious O_3 pollution threats across the coast of southern California (22). In this study, ground-level O_3 mixing ratios during the Santa Ana event increased significantly (Fig. 3*A*). The annual highest MDA8 in the Alpine station in San Diego (81 ppbv) was recorded on May 3, with a maximum 1-h O_3 mixing ratio of 88 ppbv at 1200 hours PST. Solar radiation and temperature were stronger during the Santa Ana episodes, but the ratio of NO_2 photolysis to $NO + O_3$ reaction rates ($j/k = [NO][O_3]/[NO_2]$, with the photostationary state assumption) (33) showed only slight enhancement from April 29 to May 1, suggesting that photochemical production of O_3 in the O_3–NO–NO_2 cycle was not a major factor leading to the elevated O_3 levels during the entire Santa Ana period. Although wildfires occur commonly during Santa Ana wind events, which can significantly increase ground-level O_3 mixing ratios (22, 30), no significant wildfire occurred in our study period (Fig. S1), suggesting that emissions from wildfires were also not a major contributor. A closer look into the O_3 diurnal variations reveals significant enhancements of nighttime O_3 mixing ratios during the Santa Ana period, which were 20–29 ppbv greater than on normal days (Fig. S2). Because photochemical O_3 production ceases at nighttime, this result suggests a larger contribution of long-range transports (including stratospheric intrusions) to the enhanced O_3 mixing ratios in the Santa Ana period. A negative correlation between O_3 and CO (a tracer of anthropogenic emission) may suggest O_3 originating from the stratosphere, where CO is depleted and O_3 is rich (34, 35). To rule out the potential impact of nighttime titration effect, which can also lead to negative O_3–CO correlation (36, 37), only daytime data (0700–1800 hours) were considered in this study. A significant negative correlation between O_3 and CO in the Santa Ana event ($r = -0.60$, confidence level > 99.9%) compared with normal days ($r = -0.04$, confidence level = 40.9%) implies that the elevated O_3 levels during the Santa Ana event were likely related to the vertical transport of O_3 from high altitudes.

In summary, the concurrently enhanced ground-level $^{35}SO_4^{2-}$ and O_3 concentrations and negative O_3–CO correlation indicate that the O_3 episode on May 3, 2014 was likely affected by a deep stratospheric intrusion event, a naturally occurring exceptional event. Because most Santa Ana winds only entrain air masses from the free troposphere to the boundary layer and would not lead to a significant enhancement of ground-level O_3 mixing ratios (18, 30), a stratospheric intrusion event that transports O_3-rich stratospheric air to the free troposphere before or during the Santa Ana event is required to result in the observed ground-level $^{35}SO_4^{2-}$ and O_3 concentrations. The vertical ozone profile retrieved from Global Ozone Monitoring Experiment-2 satellite observation on April 30, 2014 revealed significant enhancements of the tropopause O_3 levels and total O_3 columns at the upstream region of southern California during the Santa Ana event, indicating stratospheric air masses mixing into the troposphere (Fig. S3). Under the influences of Santa Ana winds, such O_3-rich stratospheric air may be transported downward to the boundary layer and westerly to coastal southern California.

Meteorological Model Analysis

To quantitatively estimate the probability that air masses sampled in this Santa Ana wind event partly originate from the stratosphere, an inert stratospheric tracer was simulated by a mesoscale meteorology model [Weather Research and Forecasting Model (WRF)] (20). The time series of the WRF-simulated stratospheric tracer at the boundary layer show a small peak (0.6%) at 1200 hours PST on April 30, 2014, 1 d after the onset of the Santa Ana wind event, and the highest peak (1.5%) at 0500 hours PST on May 1, 2014 (Fig. 3*C*). The WRF-simulated stratospheric tracer gradually decreased from the highest peak to baseline (~0%) from May 1 to 5, 2014 (Fig. 3*C*). Stratospheric O_3 mixing ratios at the boundary layer simulated by an independent Lagrangian particle dispersion model [FLEXible PARTicle dispersion model (FLEXPART);

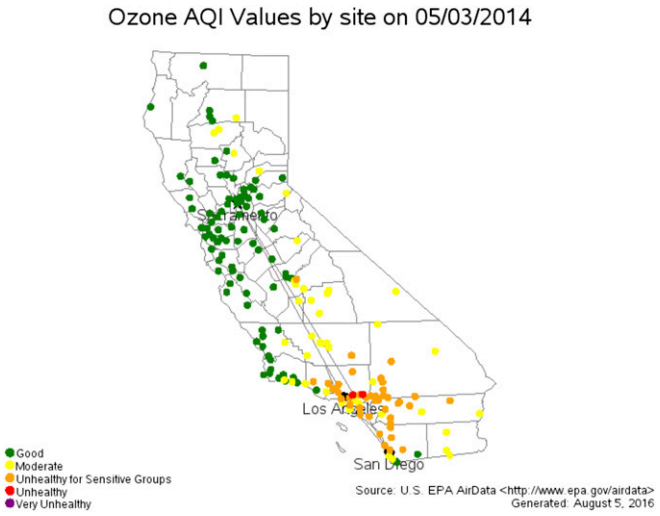

Fig. 2. Distribution of ozone AQI and levels of health concern in California recorded by the US EPA on May 3, 2014 (www3.epa.gov/airdata).

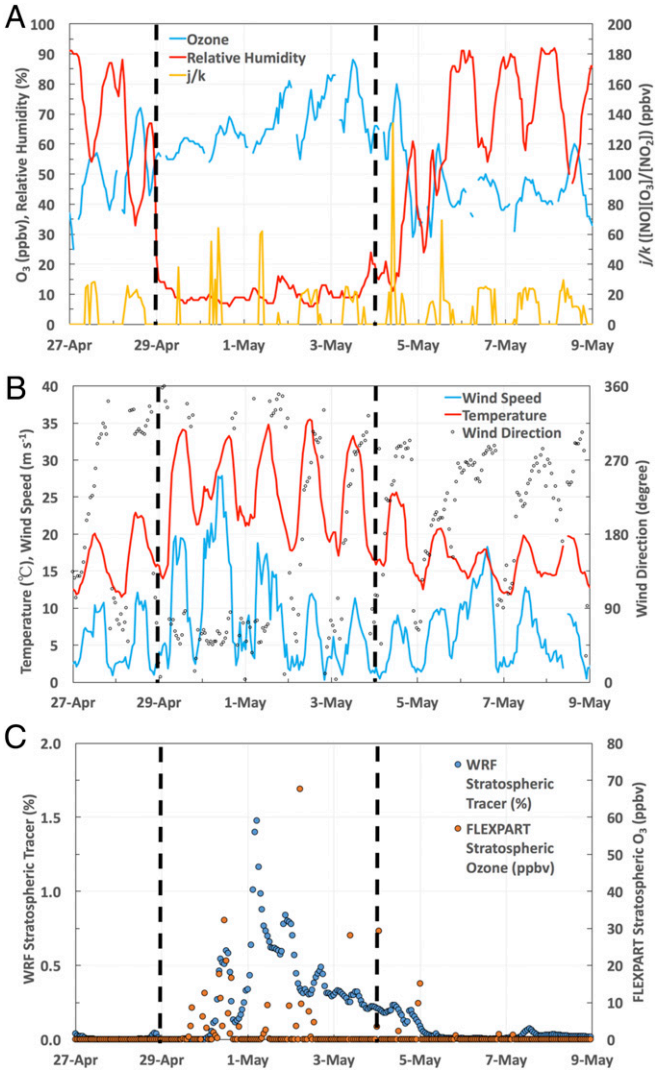

Fig. 3. Time series of hourly (*A*) O_3, RH, and *j*/*k* measured in San Diego (the Alpine monitoring station); (*B*) temperature, wind speed, and direction measured in San Diego (the Kearny Mesa station); and (*C*) the simulated WRF stratospheric tracer and FLEXPART stratospheric O_3 at the boundary layer in San Diego. The vertical black dashed lines define the period of the Santa Ana event (April 29 to May 3, 2014) based on abnormal RH and temperature.

driven by the WRF output] (19) show a consistent trend (Fig. 3*C*), further supporting the stratospheric origins of ^{35}S and O_3.

The process of how this plume intruded to the troposphere and reached coastal southern California is investigated by the horizontal distributions of the WRF-simulated stratospheric tracers and weather systems at various altitudes. As clearly shown in Fig. 4*A*, the stratospheric intrusion episode leading to the elevation of the WRF-simulated stratospheric tracer was directly triggered by a cutoff low-pressure system, which is accompanied by strong convective motions and tropopause folding and a typical synoptic condition resulting in active stratosphere to troposphere exchange over western United States (10, 22). The development of this synoptic situation is shown in Fig. S4. At the beginning, a strong midlevel short-wave trough developed into a closed low-pressure area as the system occluded over the central high plains since April 27, 2014. An associated mid- to low-level cyclone then reached its peak intensity while a trailing cold front move eastward across eastern Kansas, eastern Oklahoma, and northern Texas on April 29, 2014. Meanwhile, the strong northeasterly flow on the southwest flank of the cyclone swept through southwestern United States and caused a significant late season Santa Ana event. Later on, the low-pressure system started to abate, stretched southward from Canada to New Mexico and from northern California to the Gulf of Mexico on April 30, and eventually, dissipated after May 2, 2014.

Exchange processes between the free troposphere and the boundary layer are vital to bring ^{35}S- and O_3-rich stratospheric air to the sampling site. Fig. 4*B* shows that the impacts of stratospheric air on the boundary layer were mostly confined in the regions affected by the Santa Ana wind. Stratospheric air masses in the free troposphere started to penetrate into the boundary layer in Utah at 1000 hours PST on April 30, 2014 behind the trough line and were subsequently transported to southern California via the northeast Santa Ana wind on May 1 (Fig. S5). Zonal cross-sections of potential vorticity (PV) and the WRF-simulated stratospheric tracer clearly show the distinctive tropopause folding associated with the cutoff low between ∼105° W and ∼115° W and a tongue of stratospheric air sloping downward at ∼115° W (Fig. 5), highlighting the pathway of the stratospheric air into the boundary layer. The MDA8 O_3 mixing ratios recorded in Las Vegas (35.786° N, 115.357° W; 924 m a.s.l.), the upstream region of southern California, were 59, 69, and 56 ppbv on April 30, May 1, and May 2, 2014, respectively (airquality.clarkcountynv.gov/cgi-bin/aqi_map.pl). The increases of MDA8 on May 1 in part support our model results. Because the stratospheric air masses were continuously entrained into the free troposphere by the occluded low-pressure system, these southwestward-transported air masses might slope downward to the boundary layer in southern California as well (*SI Text* and Fig. S4).

^{35}S Box Model Calculation

Priyadarshi et al. (18) used a 1D four-box model, which was developed to calculate the $^{35}SO_4^{2-}$ concentration in fine aerosol collected at the Scripps Pier, to quantify air mixing during the Santa Ana wind events and shallow stratosphere–troposphere exchange events. The model parameters (Table S1) and uncertainties were thoroughly described in refs. 18 and 25. Specifically, it was suggested that, in a shallow stratosphere–troposphere exchange event, ∼7% of the total air masses in the free troposphere were originated in the low stratosphere per day, whereas during the Santa Ana wind event, ∼41% of air mass sampled in the marine boundary layer recently originated from the free troposphere per day (18). Here, we use the same box model and combine the mixing effects of stratospheric intrusions and Santa Ana winds (i.e., 7% × 41% = ∼3% of total air sampled in the boundary layer originated from the stratosphere in 1 d) to simulate the coupling between Santa Ana winds and stratospheric intrusions in this study. The averaged $^{35}SO_4^{2-}$ concentration during May 3–7, 2014 calculated by the model was 7,100 atoms m^{-3}, reasonably agreeing with our measurement (7,390 atoms m^{-3}). The model predicts that the averaged $^{35}SO_2$ and $^{35}SO_4^{2-}$ concentrations during the episode period (April 29 to May 3) were 2,100 and 11,000 atoms m^{-3}, respectively, which however, cannot be verified in this stage, because samples were not collected from April 29 to May 2, 2014 because of operational issues. To date, the highest $^{35}SO_2$ concentration (1,800 atoms m^{-3}) was measured at New Haven by Tanaka and Turekian (38) in April of 1992. The highest atmospheric $^{35}SO_4^{2-}$ concentration was estimated to be 15,000 atoms m^{-3} from rainwater samples as discussed previously (27). These field-based measurements suggest that our model-estimated ^{35}S concentrations during deep stratospheric intrusions are plausible. If only the mixing of stratospheric intrusion (or the Santa Ana wind) was considered, the estimated averaged $^{35}SO_4^{2-}$ concentration during May 3–7, 2014 was 3,400 (or 742) atoms m^{-3}, significantly lower than our field-based data and previous calculations, implying that the coupling between stratospheric intrusions and Santa Ana winds is crucial to lead to the observed high ^{35}S and probably, O_3 levels.

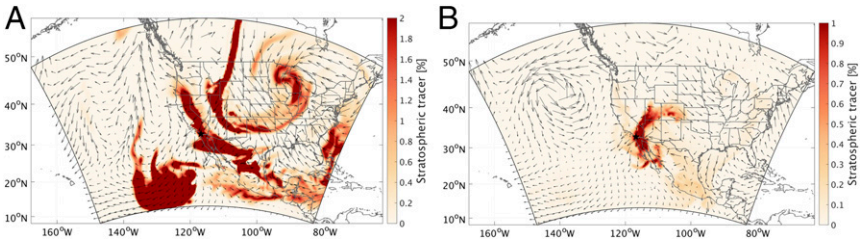

Fig. 4. Spatial distribution of the WRF stratospheric tracer at (*A*) 500 hPa at 0000 hours PST on April 30 and (*B*) 390 m above ground level at 0500 hours PST on May 1. The black star indicates the location of San Diego.

Previous studies suspected that the mixing between O_3-rich stratospheric air masses and polluted plumes might accelerate the oxidation of SO_2 (20). In this study, significant enhancements of *j*/*k* are observed during the post-Santa Ana period (May 4 and 5) (Fig. 3*A*), indicating stronger photochemical production of O_3. This phenomenon may be because the downward-transported stratospheric O_3 actively participated in the O_3–NO_x–VOCs chemistry (39, 40) when the O_3-rich air masses were mixed with polluted low-altitude air masses (41). The decreased O_3 mixing ratio (Fig. 3*A*) suggested that the photochemically produced O_3 might rapidly participate in other reactions (e.g., the formation of secondary aerosols, including heterogeneous productions of sulfate) as a sink. If the oxidation lifetime of SO_2 in the boundary layer during the post-Santa Ana period (May 4 and 5) is reduced from 4 to 0.5 d, an averaged $^{35}SO_4^{2-}$ concentration during May 3–7 of 7,400 atoms m^{-3} is obtained, perfectly matching the observational data (7,390 atoms m^{-3}). Although this hypothesis has yet to be tested by high-temporal resolution $^{35}SO_2/^{35}SO_4^{2-}$ measurement and proper chemistry modeling, the suspected enhanced aerosol formation rate is partly supported by higher $PM_{2.5}$ (particulate matter with an aerodynamic diameter less than 2.5 μm) concentrations (mean ± σ) during the post-Santa Ana period (10.8 ± 3.3 μg m^{-3}) than the Santa Ana period (6.3 ± 2.4 μg m^{-3}; 2014 annual mean: 8.1 ± 3.6 μg m^{-3}). This potential influence is particularly important in the regions heavily impacted by SO_2 emissions and stratospheric intrusions, such as East Asia (3, 20, 41, 42).

Conclusions and Implications

In summary, our result is encouraging, because it shows the high sensitivity of ^{35}S to stratospheric intrusions and reveals the crucial role of coupling between Santa Ana wind and stratospheric intrusions in bringing fresh stratospheric air to the southern California coast. The absolute amount of radiation (or activity) in the ^{35}S-rich sample is small (0.68 mBq m^{-3}) and not a concern for human health, but our highly sensitive measurement technique renders ^{35}S a sensitive tracer of stratospheric intrusions, an important process in nature for which there are gaps in understanding.

There is an urgent need to identify and screen the exceptional events for ground-level O_3 caused by stratospheric intrusions. Our study reveals that field-based measurement of cosmogenic ^{35}S at ground level can serve as an additional valuable diagnostic for the occurrence of deep stratospheric intrusions. This method has three advantages. (*i*) The optimized aerosol sample handling procedures and low-level liquid scintillation spectroscopy method enable measuring low ^{35}S activities (0.2 disintegration per minute) in a simple, economical, effective, and highly sensitive way (16). (*ii*) The half-life of ^{35}S (87 d) is ideal for studying atmospheric processes on synoptic timescales, and it also permits a relatively long storage time of aerosol samples, which are routinely collected by the EPA, until the sampling period is suspected. (*iii*) Radiogenic ^{35}S has the potential to provide additional information on the impacts of stratospheric intrusions on gas to particle conversion rates and thereafter, possible particulate matter pollution events.

Although this box model shows the ability to reproduce the observed $^{35}SO_4^{2-}$ concentration, we should mention that the box model result still possesses uncertainties, because most parameters in the model are not constrained by field-based measurements (18). The low temporal resolution of ^{35}S measurements in this study limits the use of field-based ^{35}S measurement in evaluating the model result and improving the model. In the future, a more strategic and comprehensive study can be designed to fully resolve the impacts of deep stratospheric intrusions on the tropospheric sulfur cycle and ground-level O_3 concentrations. The Realtime Air Quality Modeling System (RAQMS) model has been widely used in predicting and analyzing the stratospheric intrusion events (22, 23, 43). Although the RAQMS model underestimated the ground-level O_3 concentration in this episode (May 3, 2014), it showed capability to forecast the east Pacific storm track and stratospheric O_3 intrusions in the higher atmosphere (raqms-ops.ssec.wisc.edu/previous_products/). The forecast result of the RAQMS can be used to design intensive aerosol and SO_2 sampling for ^{35}S measurements ∼2 d before the occurrences of stratospheric intrusion events. With high temporal resolution (0.5–1 d), the evolution of ^{35}S during deep stratospheric intrusions can be resolved.

Aircraft field missions showed that concentrations of cosmogenic beryllium isotopes (^7Be and ^{10}Be; half-life = 53 d and 1.38 My, respectively) in the lower stratosphere can be ∼40–110 times greater than in the boundary layer (44, 45). Similar measurements for ^{35}S are crucial to constrain box model results. More efforts on modeling works (e.g., updating ^{35}S production rate and incorporating ^{35}S into a 3D chemistry transport model with O_3 and sulfur chemistry) can advance quantifying the impacts of stratospheric intrusions on ground-level ^{35}S and O_3 at high temporal and spatial resolutions. The extent to which stratospheric intrusions may affect the gas to particle conversion rate can also be quantified by coupled measurements of ^7Be and ^{35}S and proper modeling (38).

Climatological studies revealed that the western United States and the Himalayas are two global hotspots for deep stratospheric intrusions (4). In particular, a global chemistry–climate model showed strong contributions of stratospheric intrusions to MDA8 ground-level O_3 in Nevada (6, 7, 10). Our previous measurements showed high ^{35}S concentrations in the San

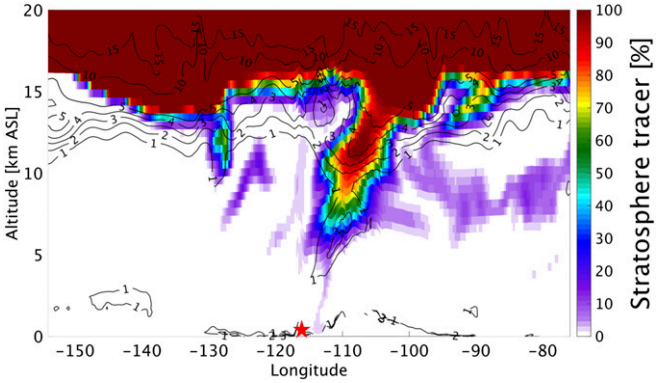

Fig. 5. Zonal cross-section of the WRF stratospheric tracer with PV (unit: PV unit) contours superimposed at 0000 hours PST on May 1, 2014. The red star indicates the location of San Diego.

Fernando Valley in California (a sampling site close to Nevada) (16) and at Mount Everest in the Himalayas (19), supporting the model results. These measurements imply that the spatial distribution of ^{35}S may provide invaluable information on regional variabilities of stratospheric intrusion strength and frequency to constrain model results. The high sensitivity of ^{35}S also allows for precise quantification of the contribution of aged stratospheric air to the background troposphere, which is crucial in understanding the O_3 budget (3, 7), the carbon cycle (46, 47), and the variations of other cosmogenic radionuclides, such as ^{10}Be, a primary proxy archive of past changes in solar activity, cosmic rays, and geomagnetic field intensity (45).

Materials and Methods

Size-segregated aerosol samples were collected using a high volume air sampler (HVP-4300AFC; Hi-Q) operated at a flow rate of ~1.13 m^3 min^{-1}. Soluble sulfate extracted from glass-fiber filter papers was subject to ^{35}S analysis using an ultralow-level liquid scintillation counting spectrometer (Wallac 1220 Quantulus) technique (16). Data on air pollutants (O_3, NO_2, NO, CO, and $PM_{2.5}$) and meteorological variables (temperature, RH, solar radiation, wind speed, and direction) were provided by the Air Pollution Control District County of San Diego (www.sdapcd.org). Field-based measurements were supported by a mesoscale meteorology model (the WRF), which permitted investigations of stratospheric intrusion processes (20). Detailed sampling, chemical processing, quality assurance, and control procedures as well as modeling approach can be found in *SI Text* and Figs. S6 and S7.

ACKNOWLEDGMENTS. We thank Dr. J. Hill-Falkenthal for helpful discussion on ^{35}S data and T. Jackson and R. Thomas for helping in sampler setups. Two anonymous reviewers are acknowledged for their valuable comments that helped to improve the manuscript. This study was supported, in part, by National Science Foundation Atmospheric Chemistry Division Grant AGS1259305 (to R.S. and M.H.T.). M.L. acknowledges Guangzhou Elite Project Fellowship JY201303.

1. McGrath JM, et al. (2015) An analysis of ozone damage to historical maize and soybean yields in the United States. *Proc Natl Acad Sci USA* 112(46):14390–14395.
2. Arneth A, et al. (2010) Terrestrial biogeochemical feedbacks in the climate system. *Nat Geosci* 3(8):525–532.
3. Verstraeten WW, et al. (2015) Rapid increases in tropospheric ozone production and export from China. *Nat Geosci* 8(9):690–695.
4. Skerlak B, Sprenger M, Wernli H (2014) A global climatology of stratosphere-troposphere exchange using the ERA-Interim data set from 1979 to 2011. *Atmos Chem Phys* 14(2):913–937.
5. Huang J, et al. (2015) Origin of springtime ozone enhancements in the lower troposphere over Beijing: In situ measurements and model analysis. *Atmos Chem Phys* 15(9):5161–5179.
6. Lin MY, et al. (2012) Springtime high surface ozone events over the western United States: Quantifying the role of stratospheric intrusions. *J Geophys Res Atmos* 117(D21):D00V22.
7. Lin M, et al. (2015) Climate variability modulates western US ozone air quality in spring via deep stratospheric intrusions. *Nat Commun* 6:7105.
8. Langford AO, et al. (2012) Stratospheric influence on surface ozone in the Los Angeles area during late spring and early summer of 2010. *J Geophys Res Atmos* 117(D21):D00V06.
9. Stohl A, et al. (2003) Stratosphere-troposphere exchange: A review, and what we have learned from STACCATO. *J Geophys Res Atmos* 108(D12):D00V06.
10. Langford AO, et al. (2015) An overview of the 2013 Las Vegas Ozone Study (LVOS): Impact of stratospheric intrusions and long-range transport on surface air quality. *Atmos Environ* 109:305–322.
11. Cristofanelli P, et al. (2010) Tropospheric ozone variations at the Nepal Climate Observatory-Pyramid (Himalayas, 5079 m a.s.l.) and influence of deep stratospheric intrusion events. *Atmos Chem Phys* 10(14):6537–6549.
12. Kuang S, et al. (2012) Stratosphere-to-troposphere transport revealed by ground-based lidar and ozonesonde at a midlatitude site. *J Geophys Res Atmos* 117(D18): D18305.
13. Cooper OR, et al. (2005) Direct transport of midlatitude stratospheric ozone into the lower troposphere and marine boundary layer of the tropical Pacific Ocean. *J Geophys Res Atmos* 110(D23):D23310.
14. Chan CY, et al. (2004) Vertical profile and origin of wintertime tropospheric ozone over China during the PEACE-A period. *J Geophys Res Atmos* 109(D23):D23S06.
15. Lal D, Peters B (1967) Cosmic ray produced radioactivity on the earth. *Kosmische Strahlung II/Cosmic Rays II*, ed Sitte K (Springer, Berlin), pp 551–612.
16. Brothers LA, et al. (2010) Optimized low-level liquid scintillation spectroscopy of 35S for atmospheric and biogeochemical chemistry applications. *Proc Natl Acad Sci USA* 107(12):5311–5316.
17. Priyadarshi A, Dominguez G, Savarino J, Thiemens M (2011) Cosmogenic S-35: A unique tracer to Antarctic atmospheric chemistry and the polar vortex. *Geophys Res Lett* 38(13):L13808.
18. Priyadarshi A, Hill-Falkenthal J, Coupal E, Dominguez G, Thiemens MH (2012) Measurements of S-35 in the marine boundary layer at La Jolla, California: A new technique for tracing air mass mixing during Santa Ana events. *J Geophys Res Atmos* 117(D8):D08301.
19. Lin M, et al. (2016) Resolving the impact of stratosphere-to-troposphere transport on the sulfur cycle and surface ozone over the Tibetan Plateau using a cosmogenic S-35 tracer. *J Geophys Res Atmos* 121(1):439–456.
20. Lin M, et al. (2016) Unexpected high S-35 concentration revealing strong downward transport of stratospheric air during the monsoon transitional period in East Asia. *Geophys Res Lett* 43(5):2315–2322.
21. Sprenger M, Wernli H (2003) A northern hemispheric climatology of cross-tropopause exchange for the ERA15 time period (1979-1993). *J Geophys Res Atmos* 108(D12): 8521.
22. Langford AO, Pierce RB, Schultz PJ (2015) Stratospheric intrusions, the Santa Ana winds, and wildland fires in Southern California. *Geophys Res Lett* 42(14): 6091–6097.
23. Baylon PM, Jaffe DA, Pierce RB, Gustin MS (2016) Interannual variability in baseline ozone and its relationship to surface ozone in the western U.S. *Environ Sci Technol* 50(6):2994–3001.
24. Cooper OR, Langford AO, Parrish DD, Fahey DW (2015) Atmosphere. Challenges of a lowered U.S. ozone standard. *Science* 348(6239):1096–1097.
25. Priyadarshi A, Dominguez G, Thiemens MH (2011) Evidence of neutron leakage at the Fukushima nuclear plant from measurements of radioactive 35S in California. *Proc Natl Acad Sci USA* 108(35):14422–14425.
26. Oltmans SJ, et al. (2004) Tropospheric ozone over the North Pacific from ozonesonde observations. *J Geophys Res Atmos* 109(D15):D15S01.
27. Cho HM, Hong YL, Kim G (2011) Atmospheric depositional fluxes of cosmogenic S-35 and Be-7: Implications for the turnover rate of sulfur through the biosphere. *Atmos Environ* 45(25):4230–4234.
28. Priyadarshi A, et al. (2013) Detection of radioactive S-35 at Fukushima and other Japanese sites. *J Geophys Res Atmos* 118(2):1020–1027.
29. Chan LY, Chan CY, Qin Y (1998) Surface ozone pattern in Hong Kong. *J Appl Meteorol* 37(10):1153–1165.
30. Bytnerowicz A, et al. (2010) Analysis of the effects of combustion emissions and Santa Ana winds on ambient ozone during the October 2007 southern California wildfires. *Atmos Environ* 44(5):678–687.
31. Sommers WT (1978) Lfm forecast variables related to Santa-Ana wind occurrences. *Mon Weather Rev* 106(9):1307–1316.
32. Cao Y, Fovell RG (2016) Downslope windstorms of San Diego County. Part I: A case study. *Mon Weather Rev* 144(2):529–552.
33. Clapp LJ, Jenkin ME (2001) Analysis of the relationship between ambient levels Of O_3, NO_2 and NO as a function of NO chi in the UK. *Atmos Environ* 35(36):6391–6405.
34. Parrish DD, et al. (1998) Relationships between ozone and carbon monoxide at surface sites in the North Atlantic region. *J Geophys Res Atmos* 103(D11):13357–13376.
35. Jiang YC, et al. (2015) Why does surface ozone peak before a typhoon landing in southeast China? *Atmos Chem Phys* 15(23):13331–13338.
36. Voulgarakis A, et al. (2011) Global multi-year O_3-CO correlation patterns from models and TES satellite observations. *Atmos Chem Phys* 11(12):5819–5838.
37. Mao HT, Talbot R (2004) O_3 and CO in New England: Temporal variations and relationships. *J Geophys Res Atmos* 109(D21):D21304.
38. Tanaka N, Turekian KK (1995) Determination of the Dry Deposition Flux of So2 Using Cosmogenic S-35 and Be-7 Measurements. *J Geophys Res Atmos* 100(D2):2841–2848.
39. Sillman S (1999) The relation between ozone, NOx and hydrocarbons in urban and polluted rural environments. *Atmos Environ* 33(12):1821–1845.
40. Meng Z, Dabdub D, Seinfeld JH (1997) Chemical coupling between atmospheric ozone and particulate matter. *Science* 277(5322):116–119.
41. Shao M, Tang XY, Zhang YH, Li WJ (2006) City clusters in China: Air and surface water pollution. *Front Ecol Environ* 4(7):353–361.
42. Lu Z, et al. (2010) Sulfur dioxide emissions in China and sulfur trends in East Asia since 2000. *Atmos Chem Phys* 10(13):6311–6331.
43. Sullivan JT, et al. (2015) Characterizing the lifetime and occurrence of stratospheric-tropospheric exchange events in the rockymountain region using high-resolution ozone measurements. *J Geophys Res Atmos* 120(24):12410–12424.
44. Jordan CE, Dibb JE, Finkel RC (2003) $^{10}Be/^{7}Be$ tracer of atmospheric transport and stratosphere-troposphere exchange. *J Geophys Res Atmos* 108(D8):4234.
45. Aldahan A, et al. (2008) Atmospheric impact on beryllium isotopes as solar activity proxy. *Geophys Res Lett* 35(21):L21812.
46. Liang MC, Tang J, Chan CY, Zheng XD, Yung YL (2008) Signature of stratospheric air at the Tibetan Plateau. *Geophys Res Lett* 35(20):L20816.
47. Thiemens MH, Chakraborty S, Jackson TL (2014) Decadal Delta O-17 record of tropospheric CO_2: Verification of a stratospheric component in the troposphere. *J Geophys Res Atmos* 119(10):6221–6229.
48. Stohl A, Hittenberger M, Wotawa G (1998) Validation of the Lagrangian particle dispersion model FLEXPART against large-scale tracer experiment data. *Atmos Environ* 32(24):4245–4264.